HHS Public Access

Author manuscript

Nat Med. Author manuscript; available in PMC 2018 December 18.

Published in final edited form as:

Nat Med. 2018 August ; 24(8): 1257–1267. doi:10.1038/s41591-018-0058-y.

Low frequency cortical activity is a neuromodulatory target that tracks recovery after stroke

Dhakshin S. Ramanathan[1,2,3,4,5,$], **Ling Guo**[1,6,$], **Tanuj Gulati**[1,7,$], **Gray Davidson**[1,2,3], **April K. Hishinuma**[1,7], **Seok-Joon Won**[1,7], **Robert T. Knight**[8,9], **Edward F. Chang**[10], **Raymond A. Swanson**[1,7], and **Karunesh Ganguly**[1,7,*]

[1]Neurology Service, San Francisco Veterans Affairs Medical Center, San Francisco, California, USA

[2]Mental Health Service, San Francisco Veterans Affairs Medical Center, San Francisco, California, USA

[3]Department of Psychiatry, University of California – San Francisco, San Francisco, California, USA

[4]Mental Health Service, VA San Diego Health System, San Diego, San Diego, California, USA

[5]Department of Psychiatry, University of California-San Diego, San Diego, California, USA

[6]Neuroscience Graduate Program, University of California – San Francisco, San Francisco, California, USA

[7]Department of Neurology, University of California – San Francisco, San Francisco, California, USA

[8]Helen Wills Neuroscience Institute, University of California, Berkeley, Berkeley, California, USA

[9]Department of Psychology, University of California, Berkeley, Berkeley, California, USA

[10]Department of Neurosurgery, University of California – San Francisco, San Francisco, California, USA

Abstract

Recent work has highlighted the importance of transient low-frequency oscillatory (LFO, < 4 Hz) activity in the healthy motor cortex (M1) during skilled upper-limb tasks. These brief bouts of

*Correspondence to: K.G. (karunesh.ganguly@ucsf.edu).
$co-first authors

Accession Codes: Not applicable.

Data availability: The datasets generated during and/or analyzed during the current study (and associated custom code) are available from the corresponding author on reasonable request.

Author Contributions: Rodent Experiments: DSR, LG, TG, SJW and KG conceived and designed the experiments. RAS provided input on design relative to stroke models. DSR, LG, TG, GD, AKH, SJW performed the experiments. DSR, LG, GD and TG analyzed the data. Human Experiments: TG, KG, EC, RTK were involved in data collection. DSR analyzed the data. DSR, LG, TG and KG wrote the manuscript. All authors contriubed to editing and revisions.

Competing Financial Interests Statement: DSR, TG and KG filed a PCT Patent Application for Systems Methods and Devices for Closed Loop Methods To Enhance Motor Recovery After Stroke.

oscillatory activity may establish the timing or sequencing of motor actions. Here we show that LFOs track motor recovery post-stroke and can be a physiological target for neuromodulation. In rodents, we found that reach-related LFOs, as measured in both the LFP and related spiking activity, were diminished after stroke and that spontaneous recovery was closely correlated with their restoration in perilesional cortex. Sensorimotor LFOs were also diminished in a human subject with chronic disability after stroke in contrast to two non-stroke subjects who demonstrated robust LFOs. Therapeutic delivery of electrical stimulation time-locked to the expected onset of LFOs was found to significantly improve skilled reaching in stroke animals. Together, our results suggest that restoration or modulation of cortical oscillatory dynamics is important for recovery of upper-limb function and that they may serve as a novel target for clinical neuromodulation.

Introduction

An emerging view of primary motor cortex (M1) sees it as an engine for movement governed by transient oscillatory dynamics present during both preparation and generation of movement [1–7]. Movement-related, low-frequency quasi-oscillatory activity (LFO), at the level of both spiking and local field potentials (LFP), has also been observed in the intact non-human primate M1 and human motor regions during reaching tasks [2–5,8–13]. Such quasi-oscillatory activity can be as brief as 1-2 cycles for rapid movements or longer during sustained movements, and appears to be closely correlated with sub-movement timing [4,5,14]. They may also be related to the multiphasic muscle activations required for precise kinetics during actions[15,16]. Thus, LFOs appear to represent an intrinsic property of motor circuits involved in the production of fast and accurate movements.

Here we hypothesized that monitoring and manipulating movement-related LFOs after stroke may offer new avenues to understand motor recovery. Prior research using invasive electrophysiological approaches has largely focused on measurements of nervous system function that occur at rest and/or away from motor tasks[17–20]. For this reason, surprisingly little is known about how stroke and recovery affects task-related neural dynamics at the level of single neurons and mesoscopic circuit function. Non-invasive studies in human subjects have found that EEG movement-related potentials (e.g. slow-cortical potentials or SCPs[21–23]) are affected by stroke[24–27]. Furthermore, changes in SCP are correlated with motor impairments post-stroke[26]. One limitation of EEG, however, is the uncertainty regarding specific anatomical generators and neural processes that contribute to the recorded potentials; moreover, SCPs include a variety of pre-movement and movement related phemonenon[22,23], further limiting their interpretation.

A generative model of cortical dynamics in both the healthy and recovering nervous system may guide the development of novel, closed-loop neuromodulatory approaches that dynamically target transient task-related processes. Despite our knowledge that neural networks are highly non-stationary, the vast majority of prior studies applying electrical or magnetic stimulation to the brain post-injury have applied it continuously, without explicitly targeting intrinsic neural dynamics[28–30] and with a primary goal of generally increasing excitability and/or plasticity[31–33]. However, recent work has suggested that therapeutic

electrical stimulation can be used to target phasic oscillatory dynamics[34,35], an idea has been successfully implemented in Parkinson's disease [36] and epilepsy [37]. Implementing such an approach post-stroke requires detailed knowledge of normal and abnormal neural dynamics, and a better understanding of how to modulate them. Here we aimed to identify neurophysiological dynamics associated with skilled execution; assess whether these same dynamics are related to recovery; and finally, to evaluate whether temporally precise electrical neuromodulation of these dynamics can improve motor function post-stroke.

Results

Long Evans male rats (n = 4) were implanted with microwire arrays in M1 after learning a skilled forelimb reach task[38] (Fig 1a-b). Animals were trained over multiple days using an automated reach-box[39]. In addition to movement-related spiking activity in M1 in well-trained rats[40,41] (Fig 1c), we also observed quasi-oscillatory low-frequency activity at the level of both LFP and spiking activity (Fig 1d, example trial; Supp Fig 1 for description of quasi-oscillatory population dynamics; Supp Fig 2a additional trial examples). We found strong movement-related power predominately in lower LFP frequencies that began prior to reach onset; neurons showed coherent spiking with the LFP at these frequencies (Fig 1e-f). We quantified these effects by calculating the mean 1.5-4 Hz LFP power and spike-field coherence or SFC (-0.25 to +0.75 s around reach onset) across channels/units from all animals. There was a significant increase in both power (mixed-effects model with 118 channels and 4 rats as random effect, $t(117) = 6.77$, $p = 5.37e\text{-}10$) and SFC (mixed-effects model with 170 units and 4 rats as random effect, $t(170) = 8.07$, $p = 1.24e\text{-}13$) during the reach as compared to the pre-reach “baseline”. Because power and SFC were computed for each trial and then averaged, these values are not related to the mean evoked “event related potential” or ERP, but rather to single-trial dynamics. Together, these findings indicate that rodent M1 also demonstrates similar task-related low-frequency quasi-oscillatory activity described in non-human-primates[2–4,14]. A dynamic increase in SFC associated with movement suggests one of two possibilities: single units and LFP could both be phase-locked to the motor action and thus simply appear phase-locked to each other; or, by contrast, there may be independent phase-locking between units and LFP. One approach of teasing this apart is to subtract out the average ERP, which represents the dominant “phase-locked” LFP activity across trials, and then recalculate power/SFC. By subtracting the ERP, we were left with “induced” oscillations (the non-phase-locked changes in power associated with movement); thus, the subsequent SFC measure indicates a more direct relationship between LFP phase and spiking that is less contaminated by phase-locked LFP activity to the reach. Using this approach, we again found a strong increase in task-evoked low-frequency SFC (Supp Fig 2b) and power (Supp Fig 2c) evoked by reaching.

One advantage of LFP recordings over spiking is stability over long-time periods[14,42,43]. In contrast, spike recordings are easily affected by micro-motion, making it difficult to follow the same ensemble across days. Notably, we found remarkable stability in the measured task-related low frequency LFP power across trials and days (Supp Fig 2d-f). Finally, LFP measurements provide information about mesoscale organization of neural activity (Fig 1g)[8,44]. Interestingly, we found that only a subset of channels demonstrated an increase in

task-related low frequency power; there appeared to be spatial clustering of channels, suggesting that M1 activation is not uniform at the mesoscale level.

After collecting electrophysiological data in the healthy state (Fig 1), we performed a distal MCA-occlusion stroke on these same animals (Fig 2a). Induction of this type of stroke could be performed without perturbing implanted electrodes, thus allowing for a direct comparison of neural activity pre/post stroke in the same animals and cortical region. The distal-MCA model stroke resulted in a large area of damage within sensorimotor cortex (Fig 2b, Supp Fig 3a). Animals were tested again after at least a 5-day rest post-stroke; neural activity was measured again once animals could attempt reaches and at least occasionally retrieve the pellet (Supp Fig 3b shows example hand trajectories). The stroke resulted in impaired skilled motor function (Fig 2c). Importantly, neural probes were positioned such that at least some electrodes remained in viable tissue (Fig 2b, Supp Fig 3a); even post-stroke, single units remained on a subset of electrodes (Fig 2d). There were fewer units post-stroke (average of 1.45 vs. 0.453 units/channel pre vs. post-stroke), but those that remained continued to demonstrate task-related increases in activity, though demonstrating significantly less modulation on average (Fig 2d, Supp Fig 3c-d). Reach-related LFOs were perturbed (Fig 2e-i). Low-frequency SFC was reduced after stroke (Fig 2g, mixed effects model $t(221) = 7.45$, $p = 2.07e\text{-}12$; Supp Fig 3e-f); changes in firing rate could not explain the observed changes in SFC (Supp Fig 3g-h). To further probe the relationship between spiking activity and LFP using a method that is not confounded by potential changes in firing rate, we calculated the preferred phase of spiking. We found strong phase-locking to the trough of the low frequency LFP pre-stroke, and no preferred phase of spiking post-stroke (Supp Fig 3i-j). LFP power also reduced after stroke (Fig 2h-i, mixed-effects model $t(100) = 6.01$, $p = 3.06e\text{-}8$; Supp Fig 3k-l). As task-related units were present, the loss of the reach-related LFP power was not simply a product of probes being in infarcted tissue (Fig 2i). The decrease in LFP power was also not due to changes in movement speed; power was not correlated with movement duration (Supp Fig 3m). As before, subtracting the mean ERP to isolate "induced" activity did not significantly change results (Supp Fig 3n-q). Together, these analyses clearly demonstrated that stroke resulted in a striking loss of LFOs and phase-locked quasi-oscillatory spiking activity.

Having observed a clear decrease in LFOs in M1 after stroke, we next wondered if recovery of function might be associated with its restoration in peri-lesional cortex. Because of variability in the location of damage after distal MCA occlusion[45], we performed this next set of experiments using a focal photothrombotic stroke model[46] to generate a relatively reproducible area of damage (Supp Fig 4a); hence allowing us to know *a priori* the location of the perilesional cortex and to target neural probes to the appropriate rostral location where rehabilitation-induced plasticity has been shown to occur[17,47]. Immediately after stroke induction, a 16 or 32-channel microelectrode array was implanted anterior to the site of the injury[48] (Fig 3a-b). Animals were given 5 days to recover from the stroke and electrode implantation; they then underwent motor training on the same task to assess the relationship between recovery and task-related LFOs in perilesional cortex. Injury resulted in impaired motor performance (73.6% ± 12.21% vs. 35.1% ± 11.9%, 2-tailed paired t-test, $t(5) = 3.35$, $p = 0.0204$) which improved over the course of subsequent training (69.1% ± 9.01% last

session; 2-tailed paired t-test comparing first vs last session, t(5) = 3.03, p = 0.0290; Fig 3c, see Supp Fig 4b for example paw trajectories).

With recovery of function, spiking activity in perilesional cortex became sharper, more task-related and more similar to that observed in the healthy M1 (Fig 3d, Supp Fig 4c-d). There was a clear emergence of low-frequency task-related activity in both spiking and LFP in perilesional cortex (Fig 3e-k). This increase in LFO can be observed in single trial examples (Fig 3e) and across trials/sessions within the same animals (Fig 3f). Statistically, there was a strong increase in 1.5-4Hz SFC (Fig 3g-h, mixed effects model t(387) = 8.94, p = 1.59e-17; Supp Fig 4e). Changes in SFC could not be explained by changes in firing rate (Supp Fig 4f-i). 1.5-4 Hz power also increased significantly (Fig 3i-j, mixed effects model t(175) = 3.11, p = 0.00217; Supp Fig 4j-k). Moreover, subtracting the ERP did not change the results (Supp Fig 4l-o).

There was a significant positive relationship between the restoration of low-frequency power and improvements in accuracy on the task (Fig 3f, example animal; Fig 3l, all animals, Pearson's correlation r = 0.576, p = 1.18e-7). There was also a significant correlation between the restoration of SFC and recovery of function (r = 0.554, p = 4.60e-7) and between single unit modulation change and recovery (r = 0.561, p = 3.01e-7). A multi-variate linear regression model with all three variables significantly predicted motor improvements (r = 0.737, p = 1.28e-11). Each variable had significant partial correlation (r = 0.428, p = 2.21e-4 for power; r = 0.339, p = 0.00410 for SFC; r = 0.398, p = 6.29e-4 for unit modulation), suggesting that all variables could independently account for variance in recovery of function.

We next assessed whether our observed phenomena in rodent models were relevant in human stroke[46] by reanalyzing invasive human ECoG (ElectroCortiocoGraphy) data collected from three human subjects undergoing invasive epilepsy monitoring to identify seizure foci[8,44]. Physiological data were recorded during a center-out reach task in which subjects were instructed to wait for a start cue and then reach as fast as possible to a target (Fig 4a). Two of these patients had intact sensorimotor cortices (hereafter Non-Stroke or NS1/NS2); the third patient, however, had experienced an ischemic cortical stroke four years prior to the monitoring (hereafter Stroke Subject or SS) (Fig 4b). The stroke subject had persistent motor deficits involving arm and hand movements (Fugl-Meyer upper-limb score of 35). He also showed impairments in speed of execution. Reaction time from “Go” to movement onset (i.e. rise in mean EMG) was slower for the affected versus unaffected arm (reaction time of 635 ± 40 and 423 ± 72 ms, respectively, t(56) = -2.7, p = 0.009, two-tailed two-sample t-test). Similarly, the reach time from movement onset to target acquisition was longer for the affected arm (reach time of 1266 ± 58 ms vs. 914 ± 51 ms, t(56) = -4.42, p = 4.65e-5, two-tailed two-sample t-test).

For ECoG recordings from NS1/NS2, we found evidence for robust task-related LFOs centered around sensorimotor cortex (Fig 4c). The time course and pattern of this activity (Fig 4d) appeared to closely resemble that observed in rodents (Fig 1f). In the SS, however, there was a striking loss of this sensorimotor reach-related low-frequency activity (Fig 4c-e). The mean normalized 1.5-4Hz LFP power for sensorimotor electrodes (from -300ms to

+ 300ms) was significantly positive for the two non-stroke subjects: NS1, normalized mean activity 0.55± 0.2 (n = 18 SM electrodes, two-tailed one-sample t-test, t(17) = 7.16, p = 2e-6) and 0.93± .25 in NS2, (n = 16 SM electrodes, two-tailed one-sample t-test, t(15) = 5.47, p = 6.5e-5), while the stroke subject showed no significant increase in power (-0.12± 0.12, n = 91 SM electrodes, two-tailed one-sample t-test, t(90) = -1.03, p = 0.304). There was a highly significant difference in task-related low frequency power between SS and NS1/NS2. We analyzed all channels from all subjects comparing healthy vs. stroke, including subject as a factor in the model to account for differences between the two healthy subjects. Using this approach, we found a highly significant overall effect (F(2,122) = 9.80, p = 1.13e-4, and more importantly, a highly significant effect of stroke (F(1,122) = 18.76, p = 3.1e-5). It is possible these results were observed because, while in healthy subjects, the LFO was dominant near the central sulcus, in stroke, due to cortical reorganization, the LFO could be observed in other regions of the brain. Indeed, prior analyses of the data from SS demonstrated intact high-gamma activity away from the central sulcus, that were correlated with muscle synergies, suggesting functional reorganization[44]. To account for functional reorganization, we thus selected channels that showed increased activity in the high-gamma band between -300 to 300 ms prior to reach. This was performed blind to location, in an un-biased manner for all three subjects. Using this method of functional[49] rather than anatomic selection, we found overall similar results (Supp Fig 5). These results suggest that low-frequency quasi-oscillatory activity is a common electrophysiological signature of healthy motor circuit function across both rats and humans.

A key goal of this project was to assess whether we could modulate task-related oscillations and thereby develop a targeted neuromodulation approach post-stroke. Prior research has demonstrated that direct current stimulation (DCS) can modulate spiking activity [50] and on-going, carbachol-induced gamma-oscillatory dynamics[34]. It has also been recently reported that low-frequency oscillatory activity observed during ketamine anesthesia is similar to the brief, low-frequency spiking/LFP dynamics during natural reaching[3]. To study the effects of DCS *in vivo*, we analyzed the effects of DCS on M1 low-frequency oscillatory activity during ketamine anesthesia (10 rats, 11 sessions). Neural recordings during anesthesia are of substantially greater quality; we can move electrodes to optimize location near neurons and greatly increase signal to noise, a requirement for monitoring spiking during stimulation. After anesthesia induction, we implanted epidural electrodes for stimulation and M1 microwire electrodes to measure neural activity (Fig 5a). Baseline spiking/LFP activity was recorded for 15 minutes, followed by recordings during the application of a 1–5 minute long DCS (mean duration 2.909 ± 0.607 mins, mean amplitude: 106.364 ± 44.526 μA) via the epidural electrodes adjacent to the implanted recording electrodes. We found that DCS could effectively modulate ongoing LFO dynamics during ketamine anesthesia (Fig 5b-d). Specifically, DCS significantly increased LFP power in the lower frequencies (Fig 5b 1.5-4Hz LFP power, baseline 0.266 ± 0.047 and with DCS 0.314 ± 0.062; two-tailed paired t-test t(10) = -2.49, p = 0.032). DCS also generally increased phasic spiking (Fig 5c) and significantly increased 1.5-4Hz SFC (Fig 5d, SFC without DCS: 0.278 ± 0.016 and during DCS 0.316 ± 0.022; one-tailed paired t-test t(49) = -1.73, p = 0.0452). Moreover, 40% of neurons changed their firing rate significantly. More specifically, 30% increased and 10% decreased their firing rates over the baseline period. SFC analyses were performed after

controlling for any firing rate changes[51]. This was important as firing rate changed significantly for these neurons at a population level (n = 50, two-tailed paired t-test, t(49) = -2.65, p = 0.0109).

We next performed experiments to assess whether shorter pulses of DCS (<5 seconds in duration), applied directly during reaching behaviors could improve motor function after stroke. Importantly, we avoided the significantly longer duration stimulation (e.g. continuous stimulation for 5 minutes) that are known to induce long-lasting changes in excitability[31,32], as we wanted to specifically assess whether transient "on-demand" stimulation could induce behavioral improvements. For these experiments, animals underwent either a photothrombotic (n = 4) or distal-MCA (n = 3) stroke induction and were implanted with cranial screws for stimulation both anterior and posterior to the injury site (Fig 6a). Animals then underwent motor training until their level of performance plateaued (see methods); DCS was then performed. Stimulation experiments occurred between 20-150 days after the stroke, with no clear relationship between time after stroke and efficacy of stimulation. We compared the effects of stimulation with a "no-stimulation" and a "sham-stimulation" condition (Fig 6b). Using this paradigm, we found that stimulation effects were "on-demand" and did not persist across blocks, allowing us to test, daily, all three conditions (blocks of trials of no stimulation, sham-stimulation or stimulation). The order of these blocks was pseudo-randomized across days in every animal, and across sessions. We calculated the percentage improvement in accuracy for each daily stimulation and sham condition relative to the no-stimulation condition for that day, and then calculated the mean improvement across days for each animal to perform statistics. Animals showed an improvement of 73± 12% in accuracy following stimulation compared with no stimulation (one-sample, two-tailed t-test, t(6) = 6, p = 9.6e-4) and a non-significant change of -4± 5% in the sham stimulation group (one-sample, two-sided t-test, t(6) = -0.77, p = 0.47, Fig 6c). There was also a significant difference in the observed behavioral effects between the stim and sham conditions (two-tailed paired-t test, t(6) = 4.91, p = 0.003). Further analyses describing stroke-type and variation in effects across days as well as additional experiments using cathodal stimulation, are described in online methods.

We next assessed whether DCS could enhance task-related LFOs. We recorded neural signals from four post-stroke rats with persistent deficits, while they attempted the reach-to-grasp task over a total of 24 sessions (total of 1031 trials, 532 reach trials with 'Stim On' and 499 trials without DCS). Simultaneous recording of neural signals during brief epochs of stimulation is particularly challenging as the stimulation onset/offset triggers large distortions in both LFP and spiking. We thus had to substantially alter the stimulation parameters. We used significantly lower current amplitudes (81.654 ± 12.414μA vs 321.4 ± 12.2μA in behavioral experiments above), longer duration pulses (DCS pulses were typically 15 seconds long) and more distant stimulation sites to accommodate recording probe (see methods). The average z-scored 1.5-4Hz LFP power was higher during DCS trials (0.201 ± 0.076) compared to no stimulation trials (0.059 ± 0.038, t(1029) = 7.425, p = 2.361e-13, mixed effects model, Fig 6d-f). We observed a trend towards increased accuracy with DCS in this set of animals 21.069 ± 14.963% increase (one-tailed paired t-test, t(3) = −1.830, p = 0.082). The reduced efficacy was likely the result of the lower current amplitude used. Consistent with this notion is the data from our early pilot experiments (see Methods)

and in the behavior-only animals (Fig 6c) where stimulation currents of >150 μA per screw were required to observe consistent behavioral improvements.

Lastly, we designed a separate set of stimulation experiments using one second long pulses in a new group of animals to replicate the prior effect and more precisely determine the temporal relationship between electrical stimulation and the neural processes underlying reach control after stroke. More specifically, we pseudo-randomly varied the timing of stimulation onset (in blocks of 25 trials) relative to the trial onset (i.e., door opened to allow reach) (Fig 6g). Importantly, the only parameter varied was the timing of the stimulation onset relative to this cue; stimulation was delivered on all trials. Next, we calculated the ΔT between stimulation onset and the actual reach onset for each trial, thereby allowing us to precisely assess the relationship between the timing of stimulation and change in motor function. We then calculated the % accuracy for all trials at a particular ΔT by binning all trials in a window of ±50 ms around that time-point (100 ms bins). We observed a significant improvement in accuracy only when ΔT occurred between 500 - 400ms from the reach (Fig 6h, two-tailed, one-sample t-test, $t(3) = 9.035$, $p = 0.0458$, Bonferroni-Holm correction for 16 time points, also see Supp Fig 6 for individual animal traces). It is important to note that, with 1 second pulses, stimulation around this time point is likely to maximally overlap with the expected LFO (visualized on the plot, though the mean LFP trace was taken from different animals). Given the brief duration of stimulation pulses, 1 second long stimulation pulses at other times were likely to begin or end during the LFO; and, interestingly, did not appear to be beneficial. Together, our data demonstrates that DCS improved motor function in a temporally restricted manner and could enhance the LFO after stroke, suggesting a novel mechanism by which neuromodulation can work to improve motor function post-stroke.

Discussion

Our results identified low-frequency quasi-oscillatory activity as an important neurophysiological marker of skilled motor control. We found evidence of such activity at the level of neural spiking and LFP during the performance of a dexterous task in rats, and in ECoG signals in human subjects without stroke. In both rodents and humans, cortical stroke appeared to significantly disrupt low-frequency activity and its reemergence strongly tracked recovery of motor performance in rats. We also found that pulses of electrical stimulation enhanced entrainment of spiking, increased LFOs, and also improved motor performance in animals with persistent deficits. Consistent with this model, electrical stimulation was primarily effective when it started prior to and lasted through the reach, suggesting that applied electrical fields directly modulated neural dynamics linked to task execution.

There is growing literature demonstrating that quasi-oscillatory low-frequency activity can capture reach dynamics[21,22,26]; our results provide evidence that this activity is relevant during recovery as well. Are these events truly “oscillatory”, given their relatively brief nature? In this study, we used an established analytic framework[52,53] for time-frequency decomposition of motor evoked activity to assess the spectral content of evoked activity. Using these methods, we were able to: 1) quantify the relationship between spiking and LFP (i.e. SFC), (2) develop a model for how DC stimulation effects neural circuits, and (3) link

our findings with human ECoG recordings. All of this suggests that LFOs provide a useful framework for characterizing important cortical dynamics during recovery. A final point in favor of this framework is that we found significant partial correlations between behavioral improvements separately for both SFC and low frequency LFP power; this suggests that specific aspects of the oscillatory dynamics (spiking and LFP) provide independent explanatory power about motor recovery. This does raise a concern regarding the correct interpretation of the SFC. Specifically, task-evoked SFC could arise simply because both LFP and spiking are phase-locked to behavior, even if they are not directly related to each other. To address this, we subtracted the average ERP, which represents the phase-locked component of the LFP[53]; we still observed task-related increase in power and SFC, suggesting the two signals are related to each other, and not simply similarly phase-locked to behavior. Together, our results indicate that restoration of oscillatory dynamics observed both in spiking and LFP data, is important for motor recovery.

What is the possible relationship between LFOs, skilled behaviors, and motor recovery? Low-frequency oscillations can be used to decode reach-related activity[7,14] and predict spiking phase across multiple behavioral states[7,14]. Such activity is also correlated with multiphasic muscle activations and movement timing[2,4,5,14,15]. Recent work also suggests that oscillatory dynamics reflect an underlying dynamical system[2]. This prior work argues that LFOs represent an intrinsic property of motor circuits associated with precise temporal control of movements. Our findings extend this body of work by linking restoration of LFO dynamics in perilesional cortex to motor recovery. Our results directly implicate LFOs in the re-instantiation of cortical control of complex limb dynamics during reaching[17]. In our human stroke subject, persistent loss of cortical LFOs may suggest a mechanism for why reaching behaviors continued to be impaired. Of course, as we were only able to get data from one stroke patient, the generalizability of these findings remains unknown. The results need confirmation in a larger cohort. Nonetheless, given the concordance with our extensive rodent-based investigations, it is reasonable to propose that recovery of LFOs may represent a marker of restored circuit dynamics after stroke important for skilled reaching.

The exact origin of LFOs and underlying generators remains unknown. While our finding that a focal cortical stroke can perturb LFOs might indicate a local source, it is also increasingly clear that local perturbations can affect large-scale networks[19,54]. Indeed, reach-related LFOs may involve striatal [55] or thalamocortical activity [56]; with impairments and recovery after stroke a function of network plasticity rather than local effects restricted to M1. It is possible that these LFOs are related to slow-cortical potentials associated with actions measured using EEG[22]. However, because those potentials may involve multiple cortical/subcortical networks, it is difficult to directly compare to our observed phenomenon. Further work specifically probing interactions between perilesional cortex and the broader motor network can clarify what drives our observed electrophysiological changes during recovery.

We found that pulses of DC stimulation (i.e. Fig 6) could improve motor function when timed to start prior to and last through the reach period. How might electrical stimulation improve motor function after stroke; and how does this differ from prior neuromodulation methods in stroke [29,30,33,57]? In many prior animal and human studies (best exemplified in

the EVEREST trial[30]), sub-threshold high-frequency epidural stimulation over perilesional cortex was used to generally enhance cortical plasticity. Stimulation was delivered for an extended period of time in an 'open-loop' manner, i.e. not-timed with behavior, and the primary outcome measures were long-term changes in map plasticity (in animals[57]) and long-lasting changes in motor function (in both animals/humans)[30,57]. Such stimulation protocols are thought to induce lasting changes in excitability[31] that likely requires BDNF[32]. A more novel form of stimulation used a closed-loop paradigm in which stimulation in one region was linked with firing activity in different region[33], but again the primary goal was to induce long-term changes in network-plasticity. In contrast to these prior efforts, our study was designed to test whether electrical stimulation could specifically modulate the brief, movement-locked neural activity identified here and thereby improve motor function, i.e. apart from any long-term changes in cortical excitability or plasticity. Indeed, we show that brief, DC pulses can modulate movement-locked low-frequency activity and can improve motor function post-stroke. Our study, therefore, provides a theoretical basis for designing a rationale, on-demand and neurally-targeted stimulation paradigm for improving motor function. Moreover, our method of delivering stimulation (i.e. via cranial-screws) is potentially translatable as a novel class of invasive medical device. Such a device could address growing concerns that non-invasive stimulation may not reliably modulate cortex [58].

Stroke is one of the primary causes of long-term motor disability. Most current therapies, including task-specific rehabilitation training, are designed to enhance endogenous neural plasticity [59]. Here we have identified a novel neurophysiological target and tested a dynamic neuromodulation approach for improving motor function post-stroke. Moreover, because LFOs can be recorded in human subjects both non-invasively (i.e. task-evoked delta/theta power using EEG) [5] and invasively (i.e. using ECoG) [8] there is a potential path to translate our results to stroke patients. These results may provide the basis for a new generation of "smart" stimulation devices that can precisely target neuromodulation to improve motor function after stroke.

Online Methods

Animal Care and Surgery

All procedures were in accordance with protocols approved by the Institutional Animal Care and Use Committee at the San Francisco Veterans Affairs Medical Center. Adult male Long Evans rats (n = 34, 250-400g, Charles River Laboratories) were housed in a 12h:12h light: dark cycle. All surgical procedures were performed using sterile technique under 2-4% isoflurane or a ketamine/xylazine cocktail. Surgery involved cleaning and exposure of the skull, preparation of the skull surface (using cyanoacrylate), and then implantation of skull screws for referencing, stimulation and overall head-stage stability. Reference screws were implanted posterior to lambda, ipsilateral to the neural recordings. The ground screw was placed in the skull contralateral to the neural recordings and either placed posterior to lambda or over the nasal bone. For experiments involved physiological recordings, craniotomy and durectomy were performed, followed by implantation of neural probes. The postoperative recovery regimen included administration of buprenorphine at 0.02 mg/kg b.w for 2 days, and meloxicam at 0.2 mg/kg b.w. dexamethasone at 0.5 mg/kg b.w and

trimethoprim sulfadiazine at 15 mg/kg b.w for 5 days. All animals were allowed to recover for one week prior to further behavioral training.

Behavior

Animals were acclimated and then trained to plateau level of performance in a reach to grasp single pellet task before neural probe implantation. Probe implantation was performed contralateral to the preferred hand. Animals were allowed to rest for 5 days before the start of experimental/recording sessions. During behavioral assessments, we monitored the animals and ensured that body weights did not drop below 90% of the initial weight.

We used an automated reach-box, controlled by custom MATLAB scripts and an Arduino micro-controller. This setup required minimal user intervention, as described previously[39]. Each trial consisted of a pellet dispensed on the pellet tray; followed by an alerting beep indicating that the trial was beginning and then the door opening. Animals then had to reach their arm out, grasp and retrieve the pellet. A real-time “pellet-detector” using an IR detector centered over the pellet was used to determine when the pellet was moved, indicating the trial was over, and the door was closed. All trials were captured by video, which was synced with electrophysiology data using Arduino digital output. The video frame rate was 30Hz for the animals in the photothrombotic stroke electrophysiology experiments (n = 6), and 75Hz for those in the MCA stroke electrophysiology experiments (n = 4) and stimulation experiments (n = 14). Physiological data presented in this paper were generally time-locked to the onset of the reach movement. Onset of reach was determined manually from recorded video, and defined as the start of paw advancement towards the slot.

In Vivo Electrophysiology

We recorded extracellular neural activity using tungsten microwire electrode arrays (Tucker-Davis Technologies). We used either 16- or 32-channel arrays (33 μm polyamide-coated tungsten microwire arrays). Arrays were lowered down to a depth of ~ 1200 - 1500μm. In healthy animals, neural probes were centered over the forelimb area of M1[17], at 3 mm lateral and 0.5 mm anterior from bregma. In photothrombotic stroke animals, the neural probe was placed immediately anterior to the stroke site, typically centered around 3-4 mm anterior and 2.5-3 mm lateral to bregma.

Units and LFP activity were recorded using a 128-channel TDT-RZ2 system (Tucker-Davies Technologies). Spike data were sampled at 24414 Hz and LFP data at 1017.3 Hz. ZIF-clip-based analog headstages with a unity gain and high impedance (~1 Gω) were used. Threshold for spiking activity was set on-line using a standard deviation of 4.5 (calculated over a 1 minute period using the TDT-RZ2 system), and waveforms and timestamps were stored for any event that crossed that threshold. Sorting was performed using Plexon Offline Sorter v4.3.0, using a PCA-based method followed by manual inspection and sorting. We included both clearly identified single-units and multi-unit activity for this analysis (results were pooled as there were not clear differences in single and multi-unit responses). A total of 171 single and multi-units were recorded from healthy animals, 53 from those same animals post MCA stroke, 170-219 from animals after photothrombotic stroke, and 50 units in the ketamine experiment (only single units with SNR > 5.5 were used in this DC

stimulation experiment in order to minimize stimulated-related contamination of neural signals). Behavior-related timestamps (i.e., trial onset, trial completion) were sent to the RZ2 analog input channel using an Arduino digital board and synchronized to neural data.

MCA Stroke

For this procedure[60], adult rats were placed in the supine position, and a ventral cervical midline skin incision was made under the surgical microscope. Both the common carotid arteries (CCAs) were carefully isolated from the adjacent vagus nerve. The animal was then placed in the lateral position, and an incision was made over the temporalis muscle, which was then retracted. The main trunk of the left middle cerebral artery (MCA) was exposed and occluded with an AVM micro clip (Codman & Shurtleff, Inc., MA) and the CCAs was occluded using micro clamps, both for 60 minutes. After ischemia, micro clip and micro clamps were removed to restore blood flow after which the wound was sutured. This procedure has been previously shown to result in long-term loss of cortical tissue, and long-term impairments in motor cortical function [61].

Photothrombotic Stroke and Electrophysiology

After craniotomy, rose-bengal dye was injected into the femoral vein using an intravenous catheter. Next, the surface of the brain was illuminated with white light (KL-1500 LCD, Schott) using a fiber optic cable for 20 minutes. We used a 4 mm aperture for stroke induction (centered in the M1 area based on stereotactic coordinates) and covered the remaining cortical area with a custom aluminum foil mask to prevent light penetration. After induction, a probe was implanted in the perilesional cortex (PLC) immediately anterior to the stroke site[48]. The craniotomy/implanted electrodes were covered with a layer of silicone (Quiksil), followed by dental cement.

Direct Current Stimulation (DCS)

Anesthesia (Ketamine) Experiment—Animals (n = 10) were initially anesthetized using a ketamine/xylazine cocktail (85 mg/kg ketamine, and 10 mg/kg xylazine), with supplemental ketamine given ~ every 40-60 minutes as needed to maintain a stable anesthetic level, and also to maintain anesthesia at stage III characterized by predominantly slow oscillations[62];0.05 mg/kg atropine was also given separately to help decrease secretions and counteract cardiac and respiratory depression. After anesthesia and craniotomy was performed, epidural stimulation electrodes were implanted (using skull-screws embedded in the skull), in the configuration noted in Fig 5. The ground screw for this and all other stimulation experiments was implanted over the contralateral nasal bone, suggesting current flow would likely go through cortex and associated pathways in an anterior-medial direction from the site of stimulation. These screws were connected to a Multi-Channel Systems Stimulus Generator (MCS STG4000 series) to deliver direct-current stimulation. In 3 animals, ~2mm tungsten wire was placed on epidural surface in the craniotomy well instead of using skull screws to deliver the electrical stimulation. 32-ch multi-electrode arrays were implanted into Layer 5 of motor cortex (1200 – 1500 μm deep). Single-unit and LFP activity was recorded for 1 hour to ensure stability of recordings and minimize drift during stimulation experiment. Then, we recorded a base-line period of neural activity (~ 15

minutes), followed by neural activity during direct-current stimulation (typically using 10 – 100 μA currents, applied for 1 - 5 minutes).

In vivo DCS Experiments

Fixed Stimulation-Behavioral experiments: After a stroke was induced (photothrombotic n = 4 and distal-MCA n = 3), two stainless steel skull-screws were implanted 1mm anterior and posterior to the stroke site; we ensured that the electrodes were as close as possible to the stroke site and that they were located near the midline of the stroke area. Ground screw was implanted over contra-lesional nasal bone. Following a one-week recovery period animals were tested several times each week and those showing no persistent motor deficit (n = 3) were excluded from further testing. Animals were tested until their behavior was at a plateau, with reach accuracies at least > 15%. Direct-current stimulation, applied using an IZ2 stimulus isolator (TDT), was administered on both variable and fixed schedules. Stimulation was delivered on 2 screws in each animal, with a maximum stimulation amplitude of 200 μA/screw. Pilot studies in the first two animals suggested that accuracy on the skilled forelimb reach task was improved with > 150μA of current/screw; based on this pilot data, we provided at least 150μA of current/screw in all animals undergoing behavioral testing. Stimulation current was increased up to the point of tolerability by the subject; with a max amplitude of 200 μA/screw. Tolerability was defined as animals not making any observable behavioral response to the onset/offset of stimulation pulse. We tested both cathodal and anodal polarities of stimulation, as described in results and below.

The current densities used in our study appear to be less that what has been used in previous studies. For example, a 2016 study used epidural electrodes for language mapping[63]. The authors report using 5-15 mA of current delivered through 2.3 mm electrodes (area of 4.15 mm^2); this results in a current density of 2.4 mA/mm^2. Similarly, the current densities used for epidural stimulation in the Everest Trial were also comparable[30]. The study reported using currents up to 13 mA using four electrodes with 3 mm diameter. Thus, each electrode could have a density of 0.46 mA/mm^2. There are also multiple non-human primate studies using epidural stimulation. We estimate the following densities for the two example studies: 0.92 mA/mm^2 [64] & 1.41 mA/mm^2 [65]. In comparison, we used 1 mm diameters screws. We typically used between 150 - 200 μA/skull screw when delivering stimulation. Our estimated current density was 0.25 mA/mm^2. Thus, to the best of our knowledge, our current densities are comparable to those used in invasive human and non-human primate studies. Fixed stimulation (n = 7, i.e. Fig 6a-c data) began 500 ms prior to the door opening (i.e. signal of trial starting), and lasted up to 5s total (encompassing the entire reach period, with stimulation turned off after the trial ended). 30-trial blocks of stimulation “on,” “off” and “sham,” (a 200 ms pulse that ended prior to the door opening, to mimic the sensory or possible alerting effects of the stimulation onset) were counterbalanced and interleaved across days. Effects of stimulation and sham were made based on percent improvements compared to temporally adjacent no-stimulation blocks. We made a decision to randomize at the level of blocks (i.e., blocks of 30 trials; 25 trials in DC Stim with physiology experiments) rather than at the level of trials because of pilot data (in 2 animals) that there were more robust behavioral effects when randomized in this manner.

Because we performed stim/sham stim sessions across days, we also calculated the standard deviation in the percentage improvement for each animal across days to see if this differed between conditions. We did not find a significant difference between the two conditions ($t(6) = 1.37$, $p = 0.21$). We did observe improvements in performance in both stroke models with no significant differences by stroke model type ($t(5) = 1.24$, $p = 0.271$). While the above experiments were all conducted using cathodal stimulation, we found similar effects using anodal stimulation condition (anodal-stimulation showed an improvement of 60 ± 12% (one-sample t-test, $t(4) = 4.95$, $p = 0.008$, $n = 5$ animals, which included experiments performed in two of the animals used above for cathodal stimulation and 3 additional animals, all in a photothrombotic stroke model). There was no difference between anodal and cathodal stimulation on motor improvement (ANOVA, $t(10) = 0.736$, $p = 0.479$).

Joint Stimulation-Physiology Experiments: In studies combining electrophysiology and DC stimulation (Fig 6d-e, $n = 4$), we found that high stimulation currents resulted in artifacts that were difficult to remove. For this reason, we utilized smaller currents (81.654 ± 12.414 μA mean current amplitudes in these experiments vs 321.4 ± 12.2 μA in behavioral experiments above), with the primary goal of understanding whether DC stim could affect the LFO in any way. DC stimulation started 9 seconds before the door opened for the reach to start, and lasted 7 seconds after the door opened in these experiments, to minimize stim-related artifact in LFP recordings of interest ($n = 4$ rats, i.e. Fig 6d-e data). Photothrombotic stroke was used in the joint stimulation and physiological recording experiments ($n = 4$). Furthermore, since the aim was to see if LFO was boosted with DCS, in these experiments, we started these experiments immediately after stroke (after a 14 day recovery period). For all fixed stimulation DCS experiments, the stimulation screws were placed anterior/posterior to the lesion/electrodes, and the "ground screw" was placed on the contra-lateral hemisphere on the nasal bone. For the joint stimulation and physiology experiments, the stimulation screws were placed somewhat diagonally and at further distance from stroke to accommodate recording array. Thus, the fixed stimulation versus joint stimulation and recording were optimized for behavioral effects versus physiologic recordings/effects respectively.

Variable Stimulation Experiment: Variable timing stimulation (Fig 6 f-g, $n = 4$) began at six time-points with respect to door-open (-1s, -.5s, 0s, .5s, 1s, 1.5s) and lasted 1 second to ensure a spread of temporal relationships between stimulation start and reach onset (ΔT). Stimulation was delivered in blocks of 25 trials with stimulation start time consistent within-block. Animals underwent 12 random-ordered blocks each day with each time-point tested in a total of 50 trials in two non-consecutive blocks. For each trial in each animal we calculated the exact time between stimulation and reach onset (ΔT) for analysis. Data was pooled in each animal from both anodal and cathodal stimulation experiments; there was no evidence that one form of stimulation worked consistently or significantly more than the other, consistent with data from the longer-duration stimulation experiments described above. Because there is some variability between the trial start (i.e. door opening), and the actual reach onset, the exact ΔT varied quite a bit from trial to trial even in the same stim block, thus helping to increase the randomization of this experiment.

Immunohistochemistry

Rats were anesthetized and transcardially perfused with 0.9% sodium chloride, followed by 4% formaldehyde. The harvested brains were post-fixed for 24 hours and immersed in 20% sucrose for 2 days. Coronal cryostat sections (40 μm thickness) were incubated with blocking buffer (10% Donkey serum and 0.1% Triton X-100 in 0.1 M PB) for 1 hr, and then incubated with mouse anti-NeuN (1:1000; Millipore, Billerica, MA) for overnight. After washing, the sections were incubated with biotinylated anti-mouse IgG secondary antibody (1:300; Vector Lab, Burlingame, CA) for 2 hrs. Sections were incubated with avidin-biotin peroxidase complex reagents using a Vector ABC kit (Vector Labs). The horseradish peroxidase reaction was detected with diaminobenzidine and H2O2. The sections were washed in PB, and then mounted with permount solution (Fisher scientific) on superfrosted coated slides (Fisher Scientific, Pittsburgh, PA). The images of whole section were taken by HP scanner, and the microscope image was taken by Zeiss microscope (Zeiss, Thornwood, NY).

Human ECoG Experiments

We utilized data that had been collected and described in two previous manuscripts[8,44]. As previously described, these studies were conducted using a protocol approved by the UCSF CHR; all studies were conducted after obtaining informed consent from subjects. Data were collected from two subjects without stroke and one subject with documented cortical stroke. All subjects had epilepsy, and had chronic ECoG grids implanted for pre-surgical monitoring/localization of seizure. Consent and details of recordings and of the specific aspects of the behavioral paradigm in healthy subjects were previously reported here[8]; and for the stroke subject here[44]. In brief, all subjects performed a center-out reaching task, in which trials began with the appearance of a target at the center of the reach field, followed, after a variable delay, with a cue indicating subjects should perform a reach to one of 4 targets.

Data analysis

LFP/ECOG and Single-Unit Analyses—Analyses were conducted using a combination of custom-written routines in MATLAB 2015a/2017a (Math Works), along with functions/routines from the EEGLAB toolbox (http://sccn.ucsd.edu/eeglab/) and the Chronux toolbox (http://chronux.org/). Pre-processing steps for LFP/ECOG analysis included: artifact rejection (removing broken channels and noisy trials); z-scoring; and common-mode referencing using the median signal (at every time-point, the median signal across the remaining electrodes, was calculated; and this median signal was subtracted from every channel to decrease common noise and minimize volume conduction). We used median referencing rather than mean referencing to minimize the effect of channels with high noise/impedance that were not discsarded). For the joint stimulation and physiology experiments, we witnessed crosstalk between channels in two animals, and thus non-median subtracted LFP was analyzed. Filtering of data at specified frequency bands was performed using the EEGLAB function eegfilt(). Calculation of power was performed with wavelets using the EEGLAB function newtimef(). All time-frequency decompositions were performed on data on a trial by trial basis to capture the “total power” (that is, both the phase-locked, i.e.,

"evoked" and non-phase-locked, or "induced") power. To isolate and also study only the "induced" oscillatory activity, we performed a similar analysis after subtracting the mean evoked potential from the single trial data. By subtracting this out, we removed on each trial the predominant phase-locked activity in the LFP, and what remained was the "induced" activity in which power is increased in a non-phase-locked way. Channels used for ECoG analysis were chosen by locating, for each subject, the central sulcus and selecting anatomically adjacent electrodes both anterior and posterior to the central sulcus. We performed the analysis using electrodes as far ventral as the Sylvian fissure for this paper; however, we also performed an analysis in which we subsampled only the dorsal half of these electrodes from each subject presumably closer to the hand knob, and found similar results.

Statistical quantification of how stroke/recovery affected power and spike-field-coherence in rodents was calculated by taking the mean power/SFC from -0.25s to 0.75s around reach onset. Only trials where the rat managed to at least touched and knocked off the pellet were included in the analysis. In Fig 1, the baseline period is -3 to -2s relative to reach onset. In Fig 2, quantifications were made between all valid trials (at least 50) in the recording block before and after stroke. In Fig 3, comparisons were made across the first 50 and last 50 trials or the first and last recording block, for power and SFC respectively, for each animal. In humans, we used data from -0.3s to + 0.3s from reach onset across all trials performed in each subject. Calculation of spike-field coherence values was performed using the Chronux function cohgramcpt. For awake task-related experiments, SFC calculations were performed using 1s windows moving by 0.025s. For the anesthetized DCS experiments, multitaper and window parameters used for sleep-epoch analyses were utilized[51,66].

Sorted spikes were binned at 20 ms unless otherwise stated. After spikes were time-locked to behavioral markers, the peri-event time histogram (PETH) was estimated by Bayesian Adaptive Regression Splines (BARS)[67]. Unit modulation was calculated as (max-min)/(max +min) firing rate from -4 to 2.5s around reach, after spline-fitting. Gaussian process factor analysis (GPFA)[68], in Supp Fig 1, was done using DataHigh[69], with spikes from -1s to +1.5s around grasp onset.

Spike-phase histograms in Supp Fig 3 and 4 were calculated by first taking the Hilbert transform of the LFP filtered from 1.5-4 Hz, and then finding the phases of the LFP at which spikes (between -0.25 and +0.75 seconds from reach onset) occurred. For every spike-LFP pair (all spikes and LFP channels from each animal, across all 4 animals), we calculated the Rayleigh's z-statistic for circular non-uniformity, and then obtained the percentage of significant pairs ($p<0.05$).

Statistical Analysis—Parametric statistics were generally used in this study (ANOVA, t-tests, Pearson's correlation and linear regression, unless otherwise stated), implemented within either MATLAB or SPSS. Linear mixed effects model (implemented using MATLAB fitlme) was used to compare the differences in unit modulation, SFC and LFP power in Fig 1-3 and the LFP power for stimulation on and off trials in Fig 6. This model accounts for the fact that units, channels or trials from the same animal are more correlated than those from different animals, and is more stringent than computing statistical significance over all units/

channels/trials[70]. We fitted random intercepts for each rat, and reported the p-values for the regression coefficients associated with pre/post stroke, early/late recovery or stimulation on/off.

In Fig 4, we used anatomically defined sensorimotor electrodes (electrodes that laid on either side of the central sulcus), and performed an ANOVA between conditions (stroke vs. non-stroke), with subject included as an additional factor. In Figure 5, we analyzed data from only one channel in each animal (non-referenced), and calculated parametric statistics across animals (5b) or units (5d). In Figure 6, we performed parametric statistics across animals. In figure 6f-g, to calculate significance, we performed two-tailed, one-sample t-tests at each time point displayed followed by Bonferroni-Holm correction for family-wise error. To confirm the effect, using a permutation test, we performed the following analysis. For each trial in each animal we calculated the time between stimulation and reach onset (ΔT) and the accuracy (success/fail) of that trial. We then randomized the accuracies relative to the (ΔT) 1000 times for each animal, maintaining in each animal the overall distribution of times (i.e. ΔT and accuracy. Then we computed for each animal the percentage accuracy at any particular ΔT (around a window of ±50 ms); and also the 1000 surrogate (i.e., randomized) accuracy at these time points. Across animals, we then calculated the mean accuracy, and compared this to the distribution of mean accuracies across the 4 animals generated from the randomized surrogates. Significance was assigned according to 2-tailed probabilities, such that at any point in time, accuracy > or < the 97.5th percentile in either direction at that particular ΔT was assigned a significance of <0.05. The significance values derived from this approach are more conservative than p-values derived from a more standard one-sample t-test at each time point, and likewise confirmed significance of the time-point in question (-450 ms prior to reach onset).

Supplementary Material

Refer to Web version on PubMed Central for supplementary material.

Acknowledgments

This work was supported by awards from NIH NINDS (Pathway to Independence Award to TG, 1K99NS097620), A*STAR (fellowship to LG), Department of Veterans Affairs, Veterans Health Administration (VA Merit: 1I01RX001640 to KG, Career Development Award: 7IK2BX003308 to DR), and NIH NIMH (5R01MH111871 to KG); and start-up funds from the UCSF Department of Neurology to KG; and a Career Award for Medical Scientists from the Burroughs Wellcome Fund to DR (1015644). KG also holds a Career Award for Medical Scientists from the Burroughs Wellcome Fund (1009855) and an Independent Scientist Award (1K02NS093014) from the National Institute of Neurological Disorders and Stroke, National Institute of Health. This human work was also supported by a grant from the NIH (R37NS21135 to RTK).

References

1. Churchland MM, Cunningham JP, Kaufman MT, Ryu SI, Shenoy KV. Cortical Preparatory Activity: Representation of Movement or First Cog in a Dynamical Machine? Neuron. 2010; 68:387–400. [PubMed: 21040842]
2. Churchland MM, et al. Neural population dynamics during reaching. Nature. 2012; 487:51–56. [PubMed: 22722855]
3. Hall TM, de Carvalho F, Jackson A. A Common Structure Underlies Low-Frequency Cortical Dynamics in Movement, Sleep, and Sedation. Neuron. 2014; 83:1185–1199. [PubMed: 25132467]

4. Bansal AK, Vargas-Irwin CE, Truccolo W, Donoghue JP. Relationships among low-frequency local field potentials, spiking activity, and three-dimensional reach and grasp kinematics in primary motor and ventral premotor cortices. J Neurophysiol. 2011; 105:1603–1619. [PubMed: 21273313]
5. Stefanics G, et al. Phase Entrainment of Human Delta Oscillations Can Mediate the Effects of Expectation on Reaction Speed. J Neurosci. 2010; 30:13578–13585. [PubMed: 20943899]
6. Mollazadeh M, et al. Spatiotemporal Variation of Multiple Neurophysiological Signals in the Primary Motor Cortex during Dexterous Reach-to-Grasp Movements. J Neurosci. 2011; 31:15531–15543. [PubMed: 22031899]
7. Mollazadeh M, , et al. Coherency between spike and LFP activity in M1 during hand movements; 2009 4th International IEEE/EMBS Conference on Neural Engineering; 2009. 506–509.
8. Ganguly K, et al. Cortical Representation of Ipsilateral Arm Movements in Monkey and Man. J Neurosci. 2009; 29:12948–12956. [PubMed: 19828809]
9. Rickert J, et al. Encoding of Movement Direction in Different Frequency Ranges of Motor Cortical Local Field Potentials. J Neurosci. 2005; 25:8815–8824. [PubMed: 16192371]
10. Donoghue JP, Sanes JN, Hatsopoulos NG, Gaál G. Neural Discharge and Local Field Potential Oscillations in Primate Motor Cortex During Voluntary Movements. J Neurophysiol. 1998; 79:159–173. [PubMed: 9425187]
11. O'Leary JG, Hatsopoulos NG. Early Visuomotor Representations Revealed From Evoked Local Field Potentials in Motor and Premotor Cortical Areas. J Neurophysiol. 2006; 96:1492–1506. [PubMed: 16738219]
12. Sasaki K, Gemba H, Hashimoto S. Premovement slow cortical potentials on self-paced hand movements and thalamocortical and corticocortical responses in the monkey. Exp Neurol. 1981; 72:41–50. [PubMed: 7202627]
13. Hashimoto S, Gemba H, Sasaki K. Analysis of slow cortical potentials preceding self-paced hand movements in the monkey. Exp Neurol. 1979; 65:218–229. [PubMed: 233558]
14. Hall TM, Nazarpour K, Jackson A. Real-time estimation and biofeedback of single-neuron firing rates using local field potentials. Nat Commun. 2014; 5:5462. [PubMed: 25394574]
15. Flint RD, Ethier C, Oby ER, Miller LE, Slutzky MW. Local field potentials allow accurate decoding of muscle activity. J Neurophysiol. 2012; 108:18–24. [PubMed: 22496527]
16. Krasoulis A, Hall TM, Vijayakumar S, Jackson A, Nazarpour K. Generalizability of EMG decoding using local field potentials; 2014 36th Annual International Conference of the IEEE Engineering in Medicine and Biology Society; 2014. 1630–1633.
17. Ramanathan D, Conner JM, Tuszynski MH. A form of motor cortical plasticity that correlates with recovery of function after brain injury. Proc Natl Acad Sci. 2006; 103:11370–11375. [PubMed: 16837575]
18. Nudo RJ, Wise BM, SiFuentes F, Milliken GW. Neural Substrates for the Effects of Rehabilitative Training on Motor Recovery After Ischemic Infarct. Science. 1996; 272:1791–1794. [PubMed: 8650578]
19. Lim DH, LeDue JM, Mohajerani MH, Murphy TH. Optogenetic Mapping after Stroke Reveals Network-Wide Scaling of Functional Connections and Heterogeneous Recovery of the Peri-Infarct. J Neurosci. 2014; 34:16455–16466. [PubMed: 25471583]
20. Brown CE, Wong C, Murphy TH. Rapid Morphologic Plasticity of Peri-Infarct Dendritic Spines After Focal Ischemic. Stroke. 2008; 39:1286–1291. [PubMed: 18323506]
21. Rockstroh B. Slow Cortical Potentials and Behaviour. Urban & Schwarzenberg; 1989.
22. Birbaumer N, Elbert T, Canavan AG, Rockstroh B. Slow potentials of the cerebral cortex and behavior. Physiol Rev. 1990; 70:1–41. [PubMed: 2404287]
23. Preparatory States and Processes. Psychology Press; 1984.
24. Honda M, et al. Movement-related cortical potentials and regional cerebral blood flow change in patients with stroke after motor recovery. J Neurol Sci. 1997; 146:117–126. [PubMed: 9077507]
25. Kitamura J, Shibasaki H, Takeuchi T. Cortical potentials preceding voluntary elbow movement in recovered hemiparesis. Electroencephalogr Clin Neurophysiol. 1996; 98:149–156. [PubMed: 8598175]

26. Yilmaz O, Birbaumer N, Ramos-Murguialday A. Movement related slow cortical potentials in severely paralyzed chronic stroke patients. Front Hum Neurosci. 2015; 8
27. Yilmaz O, Cho W, Braun C, Birbaumer N, Ramos-Murguialday A. Movement related cortical potentials in severe chronic stroke; 2013 35th Annual International Conference of the IEEE Engineering in Medicine and Biology Society (EMBC); 2013. 2216–2219.
28. Allman C, et al. Ipsilesional anodal tDCS enhances the functional benefits of rehabilitation in patients after stroke. Sci Transl Med. 2016; 8:330re1–330re1.
29. Elsner B, Kugler J, Pohl M, Mehrholz J. Cochrane Database of Systematic Reviews. John Wiley & Sons, Ltd; 2016. Transcranial direct current stimulation (tDCS) for improving activities of daily living, and physical and cognitive functioning, in people after stroke.
30. Levy RM, et al. Epidural Electrical Stimulation for Stroke Rehabilitation Results of the Prospective, Multicenter, Randomized, Single-Blinded Everest Trial. Neurorehabil Neural Repair. 2016; 30:107–119. [PubMed: 25748452]
31. Nitsche MA, Paulus W. Sustained excitability elevations induced by transcranial DC motor cortex stimulation in humans. Neurology. 2001; 57:1899–1901. [PubMed: 11723286]
32. Fritsch B, et al. Direct Current Stimulation Promotes BDNF-Dependent Synaptic Plasticity: Potential Implications for Motor Learning. Neuron. 2010; 66:198–204. [PubMed: 20434997]
33. Guggenmos DJ, et al. Restoration of function after brain damage using a neural prosthesis. Proc Natl Acad Sci. 2013; 110:21177–21182. [PubMed: 24324155]
34. Reato D, Rahman A, Bikson M, Parra LC. Low-Intensity Electrical Stimulation Affects Network Dynamics by Modulating Population Rate and Spike Timing. J Neurosci. 2010; 30:15067–15079. [PubMed: 21068312]
35. Ali MM, Sellers KK, Fröhlich F. Transcranial Alternating Current Stimulation Modulates Large-Scale Cortical Network Activity by Network Resonance. J Neurosci. 2013; 33:11262–11275. [PubMed: 23825429]
36. Rosin B, et al. Closed-Loop Deep Brain Stimulation Is Superior in Ameliorating Parkinsonism. Neuron. 2011; 72:370–384. [PubMed: 22017994]
37. Berényi A, Belluscio M, Mao D, Buzsáki G. Closed-Loop Control of Epilepsy by Transcranial Electrical Stimulation. Science. 2012; 337:735–737. [PubMed: 22879515]
38. Whishaw IQ, Pellis SM. The structure of skilled forelimb reaching in the rat: A proximally driven movement with a single distal rotatory component. Behav Brain Res. 1990; 41:49–59. [PubMed: 2073355]
39. Wong CC, Ramanathan DS, Gulati T, Won SJ, Ganguly K. An automated behavioral box to assess forelimb function in rats. J Neurosci Methods. 2015; 246:30–37. [PubMed: 25769277]
40. Kargo WJ, Nitz DA. Improvements in the Signal-to-Noise Ratio of Motor Cortex Cells Distinguish Early versus Late Phases of Motor Skill Learning. J Neurosci. 2004; 24:5560–5569. [PubMed: 15201328]
41. Ramanathan DS, Gulati T, Ganguly K. Sleep-Dependent Reactivation of Ensembles in Motor Cortex Promotes Skill Consolidation. PLOS Biol. 2015; 13:e1002263. [PubMed: 26382320]
42. Flint RD, Wright ZA, Scheid MR, Slutzky MW. Long term, stable brain machine interface performance using local field potentials and multiunit spikes. J Neural Eng. 2013; 10:056005. [PubMed: 23918061]
43. Flint RD, Scheid MR, Wright ZA, Solla SA, Slutzky MW. Long-Term Stability of Motor Cortical Activity: Implications for Brain Machine Interfaces and Optimal Feedback Control. J Neurosci. 2016; 36:3623–3632. [PubMed: 27013690]
44. Godlove J, Gulati T, Dichter B, Chang E, Ganguly K. Muscle synergies after stroke are correlated with perilesional high gamma. Ann Clin Transl Neurol. 2016; 3:956–961. [PubMed: 28097208]
45. Gharbawie OA, Gonzalez CLR, Williams PT, Kleim JA, Whishaw IQ. Middle cerebral artery (MCA) stroke produces dysfunction in adjacent motor cortex as detected by intracortical microstimulation in rats. Neuroscience. 2005; 130:601–610. [PubMed: 15590144]
46. Carmichael ST. Rodent Models of Focal Stroke: Size, Mechanism, and Purpose. NeuroRX. 2005; 2:396–409. [PubMed: 16389304]

47. Nishibe M, Edward TR, Urban I, Barbay S, Nudo RJ. Rehabilitative Training Promotes Rapid Motor Recovery but Delayed Motor Map Reorganization in a Rat Cortical Ischemic Infarct Model. Neurorehabil Neural Repair. 2015; 29:472–482. [PubMed: 25055836]
48. Gulati T, et al. Robust Neuroprosthetic Control from the Stroke Perilesional Cortex. J Neurosci. 2015; 35:8653–8661. [PubMed: 26041930]
49. Chang EF. Towards Large-Scale, Human-Based, Mesoscopic Neurotechnologies. Neuron. 2015; 86:68–78. [PubMed: 25856487]
50. Bikson M, et al. Effects of uniform extracellular DC electric fields on excitability in rat hippocampal slices in vitro. J Physiol. 2004; 557:175–190. [PubMed: 14978199]
51. Gulati T, Ramanathan DS, Wong CC, Ganguly K. Reactivation of emergent task-related ensembles during slow-wave sleep after neuroprosthetic learning. Nat Neurosci. 2014; 17:1107–1113. [PubMed: 24997761]
52. Delorme A, Makeig S. EEGLAB: an open source toolbox for analysis of single-trial EEG dynamics including independent component analysis. J Neurosci Methods. 2004; 134:9–21. [PubMed: 15102499]
53. Makeig S, et al. Dynamic Brain Sources of Visual Evoked Responses. Science. 2002; 295:690–694. [PubMed: 11809976]
54. Corbetta M, et al. Common Behavioral Clusters and Subcortical Anatomy in Stroke. Neuron. 2015; 85:927–941. [PubMed: 25741721]
55. DeCoteau WE, et al. Oscillations of Local Field Potentials in the Rat Dorsal Striatum During Spontaneous and Instructed Behaviors. J Neurophysiol. 2007; 97:3800–3805. [PubMed: 17329629]
56. Dossi RC, Nuñez A, Steriade M. Electrophysiology of a slow (0.5-4 Hz) intrinsic oscillation of cat thalamocortical neurones in vivo. J Physiol. 1992; 447:215–234. [PubMed: 1593448]
57. Plautz EJ, et al. Effects of Subdural Monopolar Cortical Stimulation Paired With Rehabilitative Training on Behavioral and Neurophysiological Recovery After Cortical Ischemic Stroke in Adult Squirrel Monkeys. Neurorehabil Neural Repair. 2016; 30:159–172. [PubMed: 26704255]
58. Lafon B, et al. Low frequency transcranial electrical stimulation does not entrain sleep rhythms measured by human intracranial recordings. Nat Commun. 2017; 8:1199. [PubMed: 29084960]
59. Dimyan MA, Cohen LG. Neuroplasticity in the context of motor rehabilitation after stroke. Nat Rev Neurol. 2011; 7:76–85. [PubMed: 21243015]
60. Longa EZ, Weinstein PR, Carlson S, Cummins R. Reversible middle cerebral artery occlusion without craniectomy in rats. Stroke. 1989; 20:84–91. [PubMed: 2643202]
61. Rogers DC, Campbell CA, Stretton JL, Mackay KB. Correlation Between Motor Impairment and Infarct Volume After Permanent and Transient Middle Cerebral Artery Occlusion in the Rat. Stroke. 1997; 28:2060–2066. [PubMed: 9341719]
62. Friedberg MH, Lee SM, Ebner FF. Modulation of Receptive Field Properties of Thalamic Somatosensory Neurons by the Depth of Anesthesia. J Neurophysiol. 1999; 81:2243–2252. [PubMed: 10322063]
63. Taplin AM, et al. Intraoperative mapping of expressive language cortex using passive real-time electrocorticography. Epilepsy Behav Case Rep. 2016; 5:46–51. [PubMed: 27408802]
64. Plautz EJ, et al. Post-infarct cortical plasticity and behavioral recovery using concurrent cortical stimulation and rehabilitative training: A feasibility study in primates. Neurol Res. 2003; 25:801–810. [PubMed: 14669522]
65. Levy R, et al. Cortical stimulation for the rehabilitation of patients with hemiparetic stroke: a multicenter feasibility study of safety and efficacy. J Neurosurg. 2008; 108:707–714. [PubMed: 18377250]
66. Gulati T, Guo L, Ramanathan DS, Bodepudi A, Ganguly K. Neural reactivations during sleep determine network credit assignment. Nat Neurosci. 2017

Advance Online Publication

67. Wallstrom G, Liebner J, Kass RE. An Implementation of Bayesian Adaptive Regression Splines (BARS) in C with S and R Wrappers. J Stat Softw. 2008; 26:1–21. [PubMed: 19777145]

68. Yu BM, , et al. Gaussian-process factor analysis for low-dimensional single-trial analysis of neural population activity. In: Koller D, Schuurmans D, Bengio Y, Bottou L, editorsAdvances in Neural Information Processing Systems 21. Curran Associates, Inc; 2009. 1881–1888.

69. Cowley BR, et al. DataHigh: graphical user interface for visualizing and interacting with high-dimensional neural activity. J Neural Eng. 2013; 10:066012. [PubMed: 24216250]

70. Aarts E, Verhage M, Veenvliet JV, Dolan CV, Sluis S. van der A solution to dependency: using multilevel analysis to accommodate nested data. Nat Neurosci. 2014; 17:491. [PubMed: 24671065]

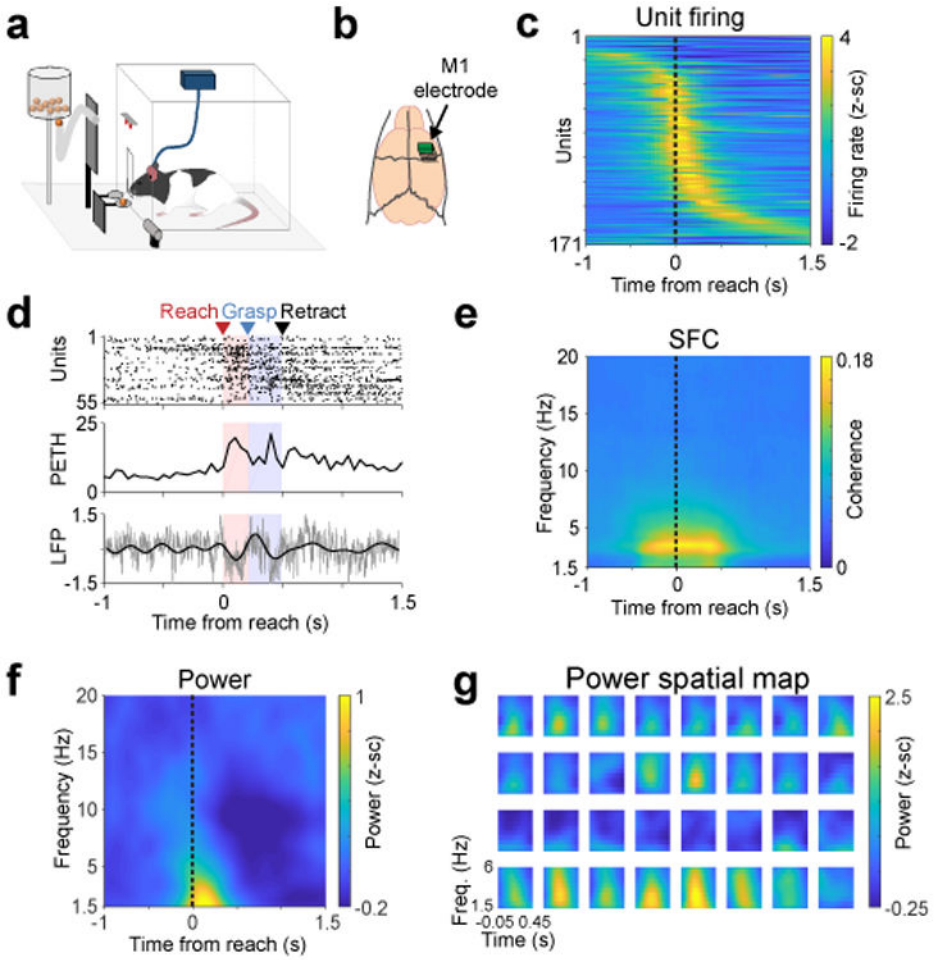

Figure 1. Low-frequency quasi-oscillatory (LFO) activity during a skilled forelimb reach task in healthy rats

a. Behavioral setup for skilled forelimb reach task with simultaneous neurophysiological recording. b. Fixed 32-channel micro-wire arrays were implanted in motor cortex. c. Z-scored firing rate changes (171 units from 4 rats) aligned to reach onset. d. Single trial example of brief low-frequency oscillatory activity during reaching (top: spike raster of all units in this example trial, middle: population peri-event time histogram for all spikes shown on top, bottom: z-scored raw LFP in gray and LFP filtered from 1.5 – 4 Hz in black from an example channel). This trial is representative example of trials that show high SFC and high power, as quantified subsequently. e. Mean spike-field coherence (SFC) across 171 units from 4 rats. f. Mean LFP power across 118 channels from 4 rats. g. 4 × 8 grid of electrodes from one animal, in actual spatial configuration, with 375 μm spacing in the y-direction and 250 μm spacing in the x-direction, plotting only power from 1.5 – 6 Hz, and from - .05 to 0.45 seconds from reach onset.

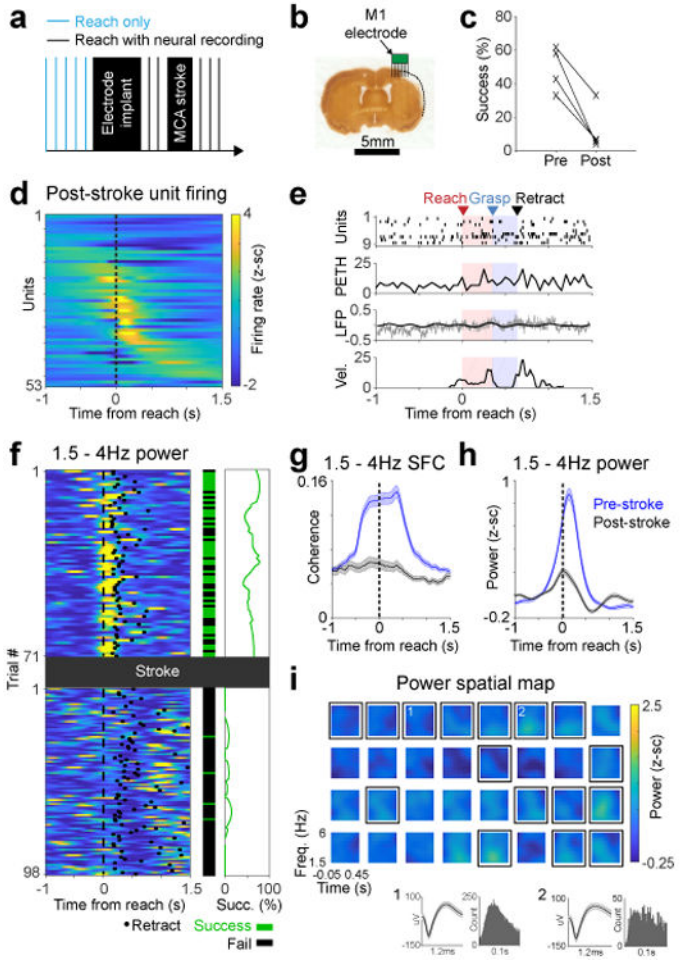

Figure 2. Stroke diminished LFO activity in M1

a. Experimental paradigm. After the MCA stroke, we continued recording neural activity from M1 during the reach task in same animals as Fig. 1. b. Histological section showing stroke and approximate location of electrodes from one animal. We performed a similar histological analysis in 4 animals to verify that there was some observable lesion resulting from the stroke. c. Pellet retrieval success rate before (mean 48.9%, SD 13.4%) and after (mean 12.4%, SD 13.8%) distal MCA stroke in 4 rats (2-sided paired t-test, $t(3) = 5.77$, $^*p = 0.010$). d. Z-scored unit firing rate changes relative to reach onset (53 units from 4 rats). e. Single trial example of diminished LFO activity. Labeling convention is the same as Fig 1d. Bottom panel shows paw velocity in arbitrary units. This is representative of trials that show low SFC and LFP power, quantified in subsequent panels (g/h) f. Trial-by-trial low frequency LFP power decrease after stroke shown in an example channel, paralleled by decrease in success rate. Left: 1.5-4 Hz LFP power, middle: trial by trial success rate, right: success rate smoothed over 25 trials. Only trials in which rat reached and touched the pellet were included. This is representative of a channel that shows high power prior to stroke and low power after, as quantified in subsequent panels (g/h) g. Quantification of 1.5-4 Hz SFC before (n = 171 units) and after (n = 53 units) stroke in 4 rats. Thick lines show mean and shaded area is SEM. h. Quantification of changes in low frequency LFP power after stroke, comparing all paired channels (n = 101) from all 4 animals. Shaded area is SEM. i. Example

grid of channels from the same rat as in Fig 1 and in the same scale. Channels with spiking activity are enclosed by black squares. Insets 1 and 2 show mean unit waveforms (shaded area is SEM) and inter-spike interval histograms from 2 selected channels. All 4 animals demonstrated a similar loss of low frequency power across channels after the stroke.

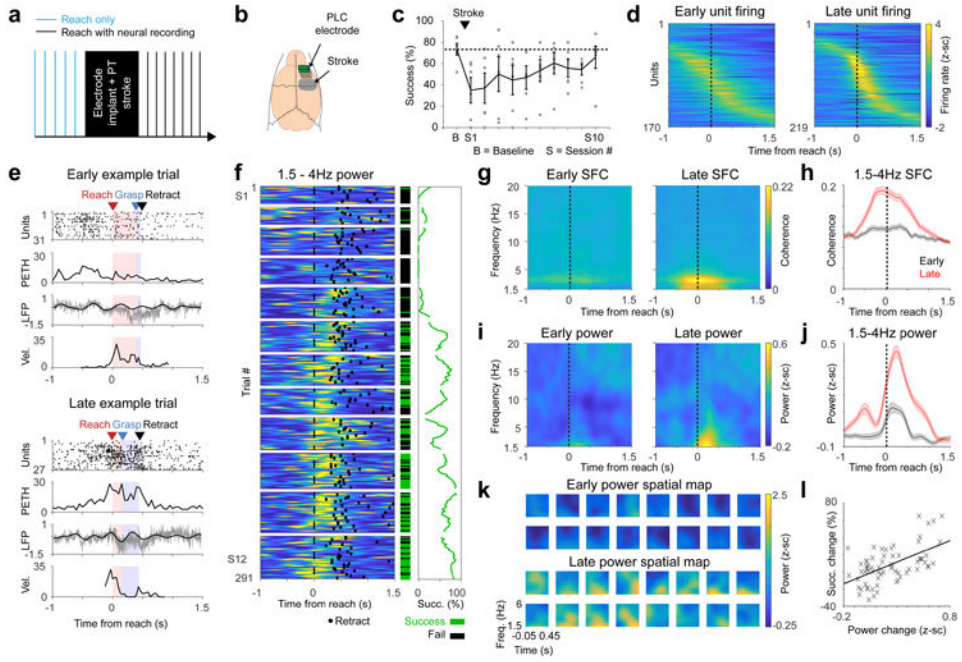

Figure 3. Restoration of LFOs in perilesional motor cortex tracked motor recovery

a. Experimental paradigm. b. Schematic showing location of stroke and electrode. c. Mean pellet retrieval success rate before stroke and during rehabilitation training sessions (n = 6, error bars show SEM, grey dots show mean of individual rats). Session 1 or S1 was 1 week post stroke for all. Each animal typically attempted 2 sessions of 25-35 trials each per day. d. Firing rate changes relative to reach onset in early (the first) and late (the last) sessions (for all units from all 6 rats). e. Example of increased LFO activity with rehabilitation, both at the level of spiking and LFP, in two trials with similar paw velocity. Labeling convention are the same as Fig 2e. f. Example channel from one animal showing trial by trial 1.5-4 Hz LFP power increase, along with success rate increase, over the course of rehabilitation training. Quantification of this effect across channels is in panels i/j. Labeling convention is the same as Fig 2f. Horizontal white lines separate training sessions. g-h. Mean SFC, calculated from units (n = 170 early, n = 219 late) in all 6 animals. Shaded area in h is SEM. i-j. Mean LFP power across channels (n = 176) from all 6 animals in early and late trials. Shaded area in j is SEM. k. Spatial topography of the low-frequency LFP power increase. Plot shows example channels from one animal. All 6 animals showed similar patterns of recovery, as quantified in panels i/j. l. Scatter showing significant correlation between restoration of low frequency power (mean 1.5-4Hz power from –0.25 to 0.75s around reach onset) and improvements on the motor task (r = 0.576, two-tailed Pearson's correlation, *p = 1.18e-7). Each x represents one session from one rat (n = 72 sessions), with values normalized for each animal to first session post-stroke.

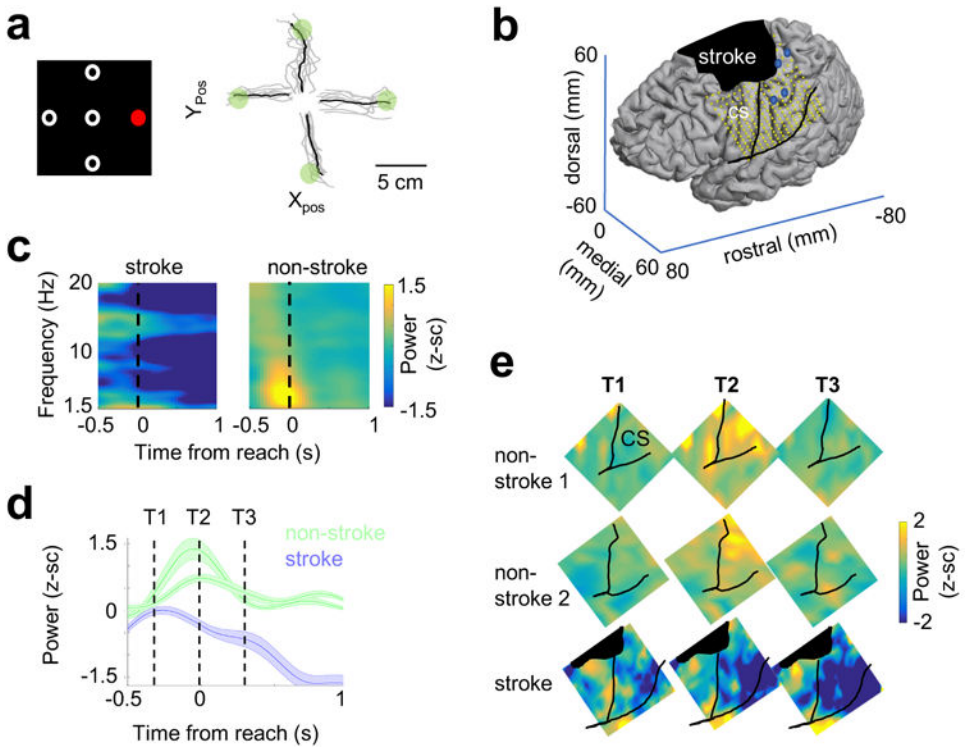

Figure 4. Movement-related LFOs in sensorimotor cortex of a human stroke patient relative to non-stroke subjects

a. Left: center-out paradigm used in patients with ElectroCorticoGraphy (ECoG) recordings. In each trial, subjects were given a hold cue, followed by a "reach" cue (red) that indicated which target to move to. Right: example of trajectories in the stroke patient. Movement-related data was recorded from 2 subjects with no stroke (NS) and 1 stroke subject (SS). Analyses were collapsed across all movement directions in each subject. b. Placement of ECoG grid in the stroke subject, and location of stroke. Blue dots on image indicate where intracortical stimulation evoked hand movements. c. Event-related spectral power across sensorimotor electrodes from one intact subject, and the stroke subject. Power normalized to a baseline time period for each channel (activity prior to the hold-cue). This experiment was not repeated on a subsequent day. d. Temporal plot of mean low-frequency power (1.5-4 Hz) from sensorimotor electrodes in each of the 2 intact subjects (NS1, n = 18 electrodes, NS2, n = 16 electrodes and the stroke subject (n = 91 electrodes). Shaded error bars display SEM for each subject across electrodes. e. Spatiotemporal plot at the 3 time-points indicated in panel (d), demonstrating increase in low frequency power along the CS (sensorimotor strip) in the two healthy subjects, and absence of this power in the stroke subject. Z-score scale displayed to the right of the image is identical for all subjects and time points. Experiments were not repeated in these subjects.

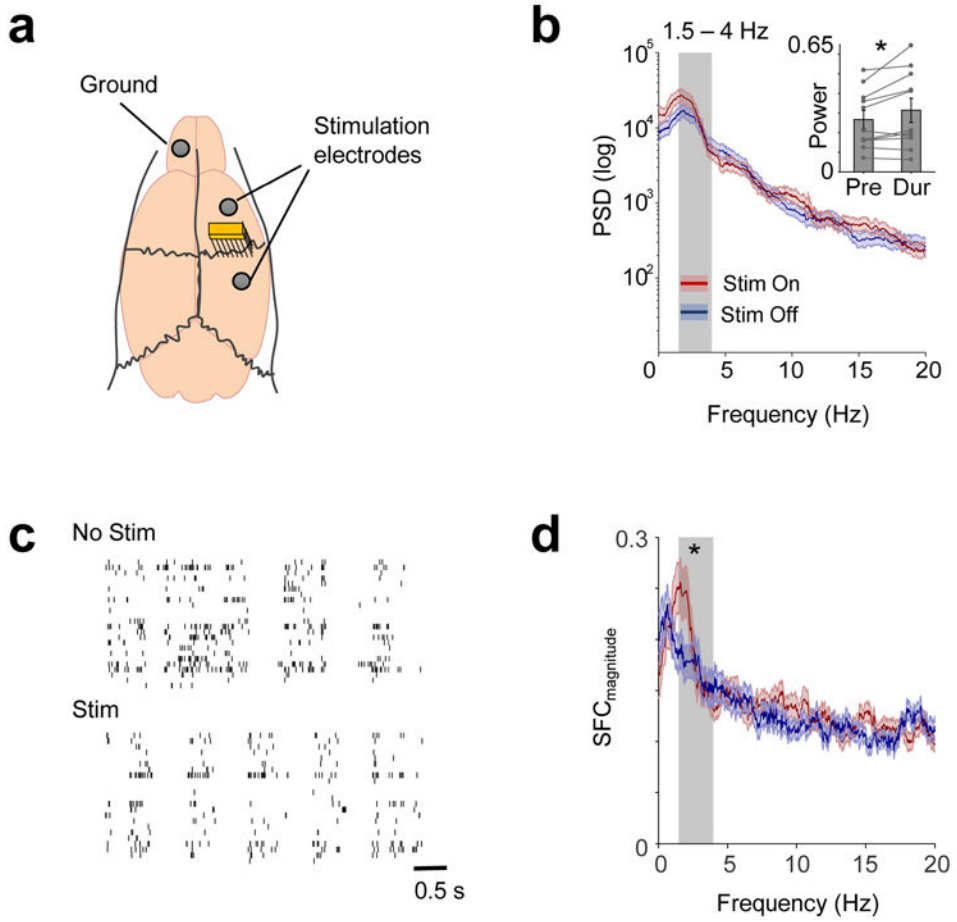

Figure 5. LFO activity increased with Direct Current Stimulation (DCS) in acute (anesthetized) recording sessions

a. Recording and stimulation arrangement in acute experiments. b. LFP power before and during DCS shown in one session. Grey shaded area shows 1.5-4Hz frequency range. Thick lines in blue and red show mean and shaded areas show SEM. Inset shows 1.5-4Hz power in pre-DCS and during-DCS in all 11 sessions from 10 rats (mean and SEM shown in bar plots with individual values, two-tailed paired t-test, t(10) = -2.493, *p = 0.032). c. Spiking activity of the same neurons from a session before and during stimulation, showing increased coherent spiking during DCS. d. Mean SFC (dark red/blue line - conventions as previous) of 50 neurons from 10 rats. Shaded area represents SEM. 1.5-4Hz SFC (grey shaded area) increased with DCS (one-tailed paired t-test, t(49) = -1.727, *p = 0.045).

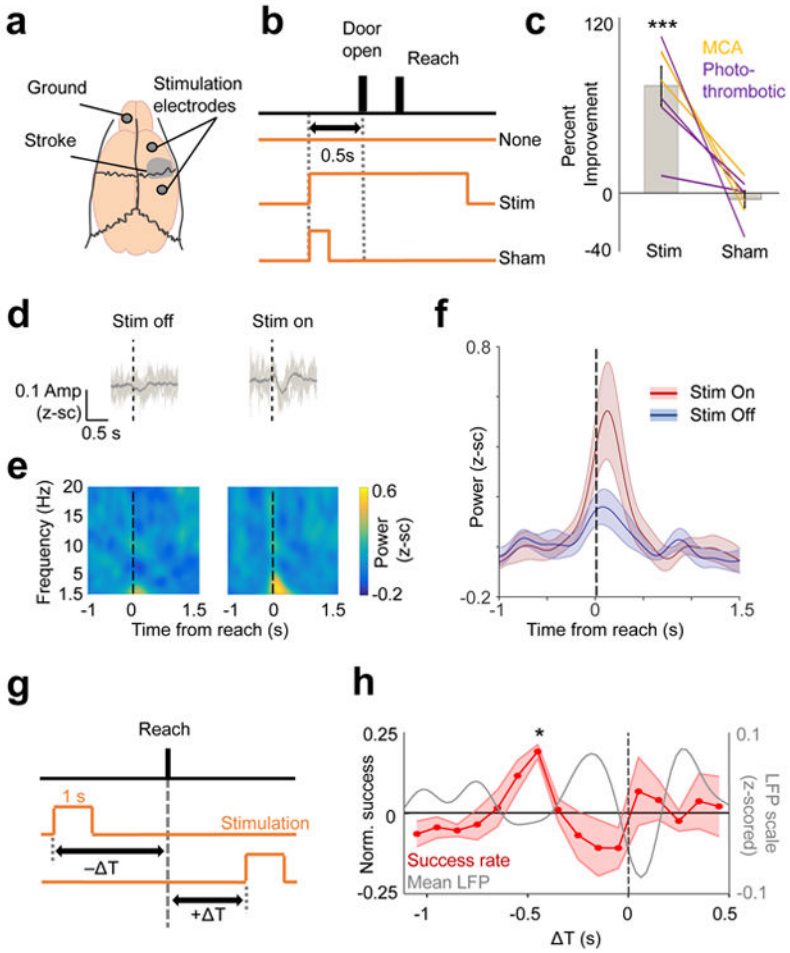

Figure 6. Task-dependent DCS improved motor function post-stroke

a. Cranial-screws placement for stimulation in relation to stroke lesion along with the ground screw. b. Pseudo-randomized stimulation design indicating the trial with either DC stimulation, a “sham-stim” control (stimulation turned on for only 200 ms), or no stimulation. c. Effects of DC vs. sham-stim on motor accuracy on the skilled forelimb reach task post-stroke. Bar plots demonstrate mean/SEM % improvement in accuracy, and lines show the effects in each animal (n = 7). We performed one-sample, two-sided t-test performed separately for the Stim ($t(6) = 6.004$, ***$p = 9.6e\text{-}4$) and Sham ($t(6) = -0.77$, $p = 0.47$) group, followed by a paired two-sample two-sided t-test to compare the effects between groups ($t(6) = 4.91$, $p = 0.003$)). d. Mean raw LFP trace (bold line, n = 70 trials stim off, n = 66 trials stim on) from one animal comparing DCS on vs. off; light grey lines show 6 example single trial traces. Dotted line indicates reach onset time. Quantification performed in next panel. e-f. Mean LFP power for all sessions (n = 13 stim on, n = 11 stim off sessions) across 4 animals. Bold line in f is the mean and the shaded area is SEM. g. Pseudo-randomized stimulation onset design depicting how a 1s stimulation was triggered in relation to reach onset. ΔT was negative if the stimulation occurred prior to reach onset, and it was positive if stimulation onset occurred after reach onset. h. Percentage accuracy as a function of ΔT (n = 4 animals). Shaded area displays SEM. (* indicates significant improvement in accuracy at ΔT between 500 - 400ms from the reach onset, $t(3) = 9.035$, *p

= 0.046, after Bonferroni-Holm correction for 16 different time points). Grey line shows the mean 1.5-4Hz LFP from healthy animals, taken from Fig 1.